Percolation picture for long wave phonons in zinc-blende mixed crystals: from (Zn, Be) chalcogenides to (Ga, In)As

2006 J. Phys.: Condens. Matter 18 577

(http://iopscience.iop.org/0953-8984/18/2/016)

INSTITUTE OF PHYSICS PUBLISHING JOURNAL OF PHYSICS: CONDENSED MATTER

J. Phys.: Condens. Matter **18** (2006) 577–595 doi:10.1088/0953-8984/18/2/016

Percolation picture for long wave phonons in zinc-blende mixed crystals: from (Zn, Be) chalcogenides to (Ga, In)As

O Pagès[1,4], T Tite[1], K Kim[2], P A Graf[2], O Maksimov[3] and M C Tamargo[3]

[1] Laboratoire de Physique des Milieux Denses, Université de Metz, 1 Bd. Arago, 57078 Metz, France
[2] National Renewable Energy Laboratory, 1617 Cole Boulevard, Golden, CO 80401, USA
[3] City College of New York, Department of Chemistry, NY 1003, USA

E-mail: pages@univ-metz.fr

Received 31 August 2005, in final form 27 October 2005
Published 14 December 2005
Online at stacks.iop.org/JPhysCM/18/577

Abstract

We propose a simplified version of the one-bond → two-mode percolation model originally developed for the long wave phonons related to the stiff Be–VI bond in (Zn, Be) chalcogenides, which open the class of random mixed crystals with contrast in the bond stiffness. This is deduced from the comparison between the Raman responses from the stiff Be–VI bond and the soft Zn–VI one in these systems. The simplified version is tested on (Ga, In)As, made of soft-like bonds only and taken here as a representative challenging system. This results in a successful reinterpretation of the puzzling multi-phonon behaviour in the Raman/infrared spectra of this alloy, that has been a subject of debate. The discussion is supported by contour modelling of the TO and LO Raman lineshapes by applying the Hon and Faust treatment to a version of the modified-random-element-isodisplacement model generalized to multi-oscillators. Also, the assignment of the long wave phonons in (Ga, In)As is supported by atomistic calculations of the bond length distributions of the minority bond species in large (Ga, In)As supercells corresponding to alloy compositions close to the In–As (In $\sim$ 0.19) and Ga–As (In $\sim$ 0.81) bond percolation thresholds. The configurations are analysed to distinguish between isolated and connected bonds, not in the usual terms of next nearest neighbours.

1. Introduction

The long wave ($q \sim 0$) phonons of $A_{1-x}B_xC$ semiconductor mixed crystals, where C defines either the cation or the anion species, are well documented both experimentally

[4] Author to whom any correspondence should be addressed.

and theoretically. It is admitted that most *random* alloys comply with the one-bond → one-mode behaviour, as envisaged by the modified-random-element-isodisplacement (MREI) model [1, 2]. Under certain conditions this also accounts for the much less frequent two-bond → one-mode behaviour, usually referred to as the mixed-mode behaviour [1, 2]. In the MREI model the alloy is artificially viewed as perfectly homogeneous at a local scale, according to the so-called virtual crystal approximation (VCA). This corresponds to a description of the whole *macroscopic* system in terms of an effective medium (EM). For example the C atoms, from the unperturbed site, are all supposed to experience the same mechanical forces produced by a statistical average of A and B nearest neighbours depending on the composition x. The VCA/EM approach is intimately associated with the concept of linearity, according to which small causes, here small variations in the alloy composition x, drive small effects in the physical properties. Accordingly, in the MREI model a single phonon frequency is naturally associated with each bond in the alloy, and each frequency is a smooth function of the composition x [1, 2].

Some well known alloys show a $q \sim 0$ one-bond → multi-phonon behaviour, which strongly deviates from the MREI picture. In particular, the complex infrared spectra from $GaAs_{1-x}P_x$ [3] and $CdS_{1-x}Se_x$ [4] were explained by assuming a local segregation effect, which refers here to site occupation preference. However, *non-random* substitution could not be verified by other techniques in these systems. More interesting is that a multi-mode behaviour was also observed in the Raman/infrared spectra from $Ga_{1-x}In_xAs$, while extended x-ray absorption fine structure (EXAFS) has shown that 'appreciable clustering on the atomic scale is absent in this zinc-blende solid solution' ([5], p 7136).

More precisely, over the past 20 years the Raman spectra from $Ga_{1-x}In_xAs$ epitaxial layers near-lattice-matched with InP ($0.32 < 1-x < 0.55$), of high technological interest, routinely showed a strong extra mode between the Ga–As and In–As bands, i.e. typically 10 cm^{-1} below the former band [6–8]. This mode occurs independently of the growth conditions and of the scattering geometries, i.e. corresponding either to allowed longitudinal (LO) or transverse (TO) optical phonons. Recently, the Raman study was extended to low In content ($0.1 < x < 0.3$) [9] and eventually to the whole composition range [10]. The extra mode is clearly visible up to $x \sim 0.55$. Its identification becomes difficult at higher x because the Ga–As and In–As bands get very close. From the separate TO and LO data available in the literature [6, 8–10], we observe that the extra mode shows up strongly in the TO symmetry, but remains weak in the LO symmetry. This has attracted little attention so far.

The origin of the extra mode in (Ga, In)As remains highly controversial. It is currently attributed to zone-edge disorder-activated TO (DATO) modes as can be explained by the spatial correlation model [11], the result of the large lattice mismatch between GaAs and InAs ($\Delta a/a \sim 7\%$). Accordingly, the Raman spectra would essentially replicate the optical-phonon density of states [10]. However, recent first-principles calculations of the phonon density of states in $Ga_{1-x}In_xAs$ performed by Branicio *et al* [12] did not show the extra mode at any composition x. A standard one-bond → one-band behaviour is observed, which does not shed light upon the three-mode behaviour observed at the zone-centre by Raman/infrared analysis.

At $x \sim 0.25$, where the extra mode shows up clearly in the Raman spectra [9, 10], it is remarkable that the extra mode and the allowed GaAs- and InAs-like LO modes undergo perfect extinction when changing from the LO-activated to the LO-extinct polarized set-ups [10]. As disorder-activated modes have little symmetry, this strongly suggests that the extra mode is an allowed zone-centre mode. As a matter of fact careful infrared analysis performed by Mintairov *et al* at $x \sim 0.25$ indicates that the extra mode consists of a zone-centre (TO, LO) doublet, even though the TO–LO splitting remains weak (~ 3 cm^{-1}) [9]. Still, at the cost of a rather intense curve-fitting procedure Mintairov *et al* observe that the TO–LO splitting enlarges with $(1-x)$, which suggests that the extra mode is due to Ga–As vibrations. We

mention that the (TO, LO) Raman spectra reported at $x \sim 0.25$ in [9] and [10] are identical. Thus, the infrared results cannot be merely fortuitous.

According to Mintairov *et al* the most likely reason for the one-bond → two-mode Ga–As behaviour is partial ordering of the solid solution [9]. Basically, the 'nominal' and extra Ga–As modes would refer to Ga–As vibrations within the dominant disordered region of the crystal and small ordered regions dispersed here and there, respectively. As a matter of fact partial atomic ordering in $Ga_{1-x}In_xAs$ was actually mentioned in some cases [13]. However, this is well known to be very dependent on the growth techniques and conditions [10], while the extra mode is not. *The problem then is to find a picture that reconciles the zone-centre character of the multi-phonon behaviour in the Raman/infrared spectra of (Ga, In)As with the generally random character of the In substitution to Ga.* This would be very challenging for the traditional MREI picture.

Precisely, our view is that the approximation of local homogeneity (VCA/EM) upon which the MREI model is based is valid mainly for band structure and lattice parameter calculations, not for vibrational properties. Indeed the former properties are integral in character, and thereby operate a natural average on alloy disorder. The electron wavefunctions of interest in the formation of the valence and conduction bands are delocalized, which obscures the detail of the atomic site potentials. Also, the lattice parameter measures the average distance between high density atomic planes, irrespective of the local bond distortions that accommodate the lattice mismatch. As a matter of fact, the bandgap and lattice parameter exhibit smooth Vegard-like dependences versus the alloy composition x in most random $A_{1-x}B_xC$ semiconductor alloys. However, this does not apply to vibrational properties because these are bond related, i.e. local in nature. Accordingly, we claim that their basic understanding requires detailed insight into the topology of the substituting species. This falls into the scope of the percolation site theory [14, 15].

Precisely, in the past few years we have developed a percolation approach for the very basic understanding of the atypical one-bond → two-mode behaviour that exhibits the stiff (Be, N)-based bond in the Raman spectra of the arriving zinc-blende alloys involving these light first row elements in substitutional position. These have small covalent radii, thus the bond length is small, which goes with increased bond stiffness. For example, replacing Zn (As) by Be (N) with Se or Te (Ga) as the anion (cation) corresponds to a reduction of ∼9% (∼20%) in the bond length, and roughly doubling (increasing fourfold) the shear (bulk) modulus [16]. While nitrides phase separate from as low N content as 2% [17], Be substitutes randomly to Zn so that very high quality (Zn, Be) chalcogenide crystals can be grown throughout the whole composition range. The percolation approach is based on the idea that the topological disorder should impart a composite hard/soft character to the (Be, N) based mixed crystals. This corresponds to a description of the mixed crystal at the *mesoscopic* scale, not at the *macroscopic* scale as with the traditional MREI model.

Regarding (Zn, Be) chalcogenides, the low and high frequency Be–VI Raman modes discriminate between vibrations within the randomly formed hard Be-rich and soft Zn-rich host regions, respectively [18–20]. Accordingly, the modes were labelled with superscripts h and s, respectively. The reason is that the Be–VI bonds from the Be-rich region, i.e. more BeVI-like, are longer than those from the Zn-rich region, i.e. more ZnVI-like (we recall that the force constant reduces with larger bond length). Recently, the latter *microscopic* mechanism for activation of the Be–Se two-mode Raman behaviour could be verified by making first-principles calculations of the internal tensions and frozen phonons in a fully relaxed prototype $Zn_{26}Be_6Se_{32}$ cell (Be content ∼0.19) containing two isolated Be atoms (Be atoms within the Zn-rich region) and four Be atoms arranged in a straight wall-to-wall chain of Be–Se bonds (Be atoms within the Be-rich region). The bond length difference (∼2%) was shown to generate

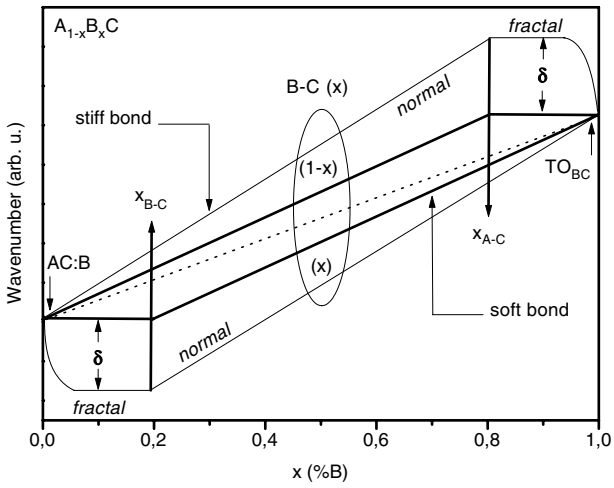

Figure 1. Schematic view of the starting one-bond → two-mode TO double branch for a *stiff* B–C bond in a random $A_{1-x}B_xC$ alloy according to the percolation picture (thin lines). This corresponds to a finite frequency gap δ out of the percolation range. For a *soft* B–C bond the corresponding double branch (thick lines) is obtained by taking δ equal to zero. This is referred to as the simplified version of the percolation model in the text. The relative strength of each TO mode within the double branch is indicated within brackets. The MREI-like one-bond → one-mode behaviour is also schematically outlined (dotted line), for reference purpose.

a phonon density of states close to the zone centre that ideally mirrors the Be–Se two-mode Raman signal from (Zn, Be)Se (Be content ∼ 0.19) [21].

The TO double branch which emerges for the stiff Be–VI bond in the reference $Zn_{1-x}Be_x$ (Se, Te) systems is schematically outlined in figure 1 (thin lines). The double branch is fully symmetrical, as ideally expected in the case of random Be substitution to Zn. The low and high frequency Be–VI TO modes scale as the scattering volumes of the hard Be-rich and soft Zn-rich host regions from which they stem, i.e. as x and $(1-x)$, respectively. It is remarkable that the bond percolation thresholds, which correspond to the first occurrences of wall-to-wall chains of the Be–VI (Be content denoted $x_{\mathrm{Be-VI}} = 0.19$) and Zn–VI bonds (Be content denoted $x_{\mathrm{Zn-VI}} = 0.81$), mark the separation between two different dynamical regimes: one in which the optical mode of the most dilute cation vibrates at a frequency that is essentially independent of the alloy composition x (regime 1), and one in which the frequency of the same mode depends smoothly on x (regime 2). Details are given elsewhere [19, 20]. In our previous Raman studies of the (Zn, Be)VI systems most of our attention was dedicated to the percolation range ($0.19 <$ Be-content < 0.81), where the two-mode behaviour of the stiff Be–VI bond shows up strongly. There, regime 2 prevails. It could be explained by using a traditional but 're-scaled' MREI model [18]. At present regime 1 remains unexplained.

We have shown that the Raman behaviour from the stiff/short Ga–N bond in the non-random Ga (As, N) [22] and (Ga, In)(As, N) [23] alloys (N ∼ 3%) basically fits in the above picture.

Now, percolation behaviours rely upon far-reaching topological effects above all else [14, 15]. Accordingly, if a percolation behaviour is observed for a given bond in a given zinc-blende alloy, then a similar behaviour is expected for every bond in every zinc-blende alloy, although the magnitudes of the percolation effects might differ from one alloy to another. As a matter of fact, recent first-principles calculations performed by Bellaiche

et al [24] regarding another bond property, i.e. the *bond length*, have shown that $GaAs_{1-x}N_x$ ($\Delta a/a \sim 20\%$) and $GaAs_{1-x}P_x$ ($\Delta a/a \sim 3\%$), ideally modelled as random systems, exhibit similar anomalies at the two-bond percolation thresholds. More interesting is that the anomaly is exacerbated for the stiff Ga–N bond, corresponding to a large bond-stretching force constant ($\sim$96 N m^{-1}) [24]. Also, the anomaly related to the soft Ga–As bond, corresponding to a much reduced bond-stretching force constant ($\sim$41 N m^{-1}) [25], is more pronounced in the alloy with the larger contrast in the bond stiffness ($\sim$57% in GaAsN, against $\sim$13% in GaAsP, see [25]).

Basically, we expect the same trend for the vibrational properties, that relate directly to the *bond force constant*. It is precisely our aim in this work to derive a general version of the percolation model that applies to the long wave phonons in the usual zinc-blende mixed crystals, i.e. made of soft-like bonds only. First our attention is focused upon the Raman response of the soft Zn–VI bond in the pioneer (Zn, Be)VI systems, in search of a possible one-bond $\rightarrow$ two-mode behaviour (section 3). This is because percolation effects are exacerbated in contrasted systems, as already mentioned. As expected, the two-mode behaviour is evidenced (section 3.1). In particular, regime 1 is also observed in the Zn–VI spectral range, which motivates a bond-independent explanation (section 3.2). Still, we identify one clear difference between the two-mode Raman responses from the stiff Be–VI bond and the soft Zn–VI one. On this basis we derive a simplified version of the percolation model for the usual mixed crystals (section 3.3). The latter version is eventually tested on (Ga, In)As, taken here as a representative challenging system (section 4). In particular the Raman lineshapes calculated via the simplified version of the percolation model are directly compared to recent (Ga, In)As data taken from the literature (section 4.1). No adjustable parameter is needed. Technically, the model results from application of the Hon and Faust formalism to a version of the MREI model generalized to multi-oscillators. Details are given elsewhere [19]. Finally, the assignment of the long wave phonons from (Ga, In)As is supported at the microscopic scale by using detailed atomistic calculations of the bond length distribution of the minority bond species in fully relaxed (Ga, In)As supercells corresponding to In contents close to the Ga–As ($\sim$0.81) and In–As ($\sim$0.19) bond percolation thresholds (section 4.2). Random In substitution to Ga is assumed. Large supercells (1728 atoms) are used with atom configurations generated at random. Basically, these are analysed to distinguish between isolated and connected bonds, as strongly suggested by the percolation picture, i.e. not in the usual terms of next nearest neighbours. Conclusions are summarized in section 5.

Generally, most of our attention is dedicated to the TO modes because these consist of purely mechanical vibrations, i.e. quasi-independent oscillators, and thereby carry clear information regarding both the strength and the frequency of the individual oscillators in the crystal. We have shown that the information is screened in LO symmetry, due to coupling via the long range polarization field [19].

2. Experiment

We use a large set of $Zn_{1-x}Be_xTe$ layers ($x \leqslant 0.3$) grown by molecular beam epitaxy on a 170 nm thick $Ga_{0.5}In_{0.5}As$ buffer lattice-matched with the underlying InP substrate. The typical layer thickness is $\sim$1 μm. The alloy composition was derived from the lattice constant measured by x-ray diffraction, by assuming a linear dependence. The difference between the lattice constants of the BeTe (5.627 Å) and ZnTe (6.089 Å) parent materials is large (7.5%), so that high accuracy is expected in the determination of the alloy composition.

Now we summarize briefly the available information concerning the crystalline quality of our (Zn, Be)Te samples. By assuming a linear dependence of the lattice constant versus the

alloy composition x, lattice-matching at the $Zn_{1-x}Be_xTe$/InP-like interface is expected around stoichiometry, i.e. $x_c \sim 0.5$. Below (above) this limit the (Zn, Be)Te epilayers should undergo a compressive (tensile) biaxial strain from the substrate during the growth process. We have realized Raman profiles along the ∼1% (100) slopes of bevelled edges realized by chemical etching with several (Zn, Be)Te epilayers covering the whole composition range. In each case we have observed that the Raman signals in the Zn–Te and Be–Te spectral ranges remain unchanged when the microprobe moves across the slope on the layer side. In particular, the extreme signals from the near-interface and the top surface ideally superimpose after proper intensity renormalization. We deduce first that the distribution of biaxial strain along the growth axis, if any, has no detectable influence upon the phonon lineshape, and second that there is no deviation from the nominal composition in the alloy as the layer grows. Indeed, we recall that the Be–Te signal is shifted by ∼100 cm^{-1} throughout the whole composition range [26], and is thereby highly sensitive to change in the (Be, Zn) content. Basically, regarding Raman analysis at least, our (Zn, Be)Te epilayers seem homogeneous in every respect.

In the present work unpolarized and unanalysed Raman spectra were recorded at room temperature in backscattering along the [110]-edge axis of each (Zn, Be)Te epilayer by taking advantage of the high spatial resolution of the Dilor XY microprobe. By using the (×100) objective the diameter of the impact spot onto the sample surface could be reduced to less than ∼1 μm. This geometry is TO allowed and LO forbidden. Most of the spectra were recorded by using the 647.1 nm excitation line from a Kr+ laser. However, at the especially sensitive composition $x \sim 0.2$ we used the more effective 488 nm Ar+ laser line in order to improve the signal-to-noise ratio in the Zn–Te range. A typical laser output of 50 mW was used, corresponding to a standard illumination of 10 MW cm^{-2} at the impact spot.

3. (Zn, Be)Te (Be content ⩽0.3): experimental results and discussion

Here we investigate in detail the TO Raman response from the soft Zn–VI bond in (Zn, Be) chalcogenides, in search of a possible one-bond → two-mode behaviour. The Zn–Se Raman signal in the reference (Zn, Be)Se system is very distorted due to strong Fano interference with disorder-activated zone-edge acoustical bands, especially in the TO symmetry [18]. As an alternative we turn to the soft Zn–Te bond in the similar (Zn, Be)Te system. Interestingly, the TO phonon in the parent material ZnTe is nearly dispersionless [27]. Therefore, even small fluctuations in the Zn–Te bond length, according to whether the Zn–Te bond belongs to the hard Be-rich region or to the soft Zn-rich one, should give rise to phonon localization, i.e. to different Raman signals corresponding to as many zone-centre modes [28]. This provides a favourable context for our purpose.

3.1. Soft Zn–Te bond: a one-bond → two-mode behaviour in the Raman spectra

We show in figure 2 representative TO Raman responses from (Zn, Be)Te within both the Zn–Te and Be–Te spectral ranges, at increasing Be content from the Be-dilute limit up to the limit of detection of the Zn–Te signal (Be content ∼0.3). On account of the small mass of Be with respect to Zn, in the ratio 1:9, and of the large stiffness of the Be–Te bond as compared to the Zn–Te one, the Zn–Te bond vibrates at much lower frequency (∼180 cm^{-1}) than the Be–Te one (∼420 cm^{-1}). Incidentally, the 488.0 nm laser excitation line preferred at $x \sim 0.2$ brings near-resonant excitation conditions, which accounts for the slight parasitical emergence of the ZnTe-like 2LO mode in the Be–Te spectral range (refer to the star in figure 2). No parasitical effect is to be feared in the spectral region of the ZnTe-like TO mode, which attracts most of our attention here. Indeed the resonance-sensitive ZnTe-like LO mode emerges at a much larger frequency, i.e. ∼205 cm^{-1} [26].

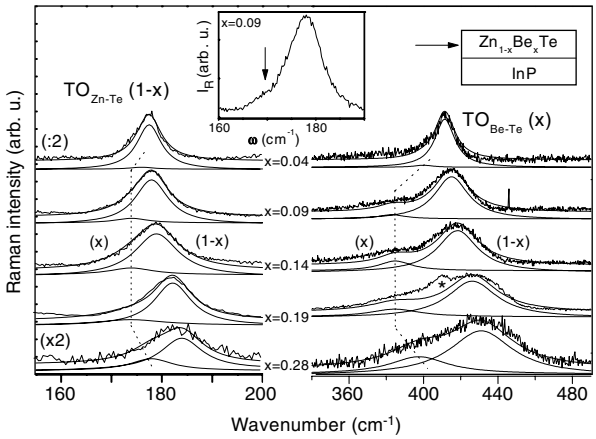

Figure 2. Raw TO Raman spectra from the $Zn_{1-x}Be_xTe$ ($x < 0.3$) alloy recorded by using the backscattering geometry along the [110]-edge axis, as schematically indicated. The TO curves are translated along the vertical axis for clarity. The multi-mode TO curves calculated by using the four-oscillator system [$(Zn–Te)^h$, $(Zn–Te)^s$, $(Be–Te)^h$, $(Be–Te)^s$] as described via the percolation model are superimposed, for comparison. The individual TO contributions are shown for a clear insight upon the (h, s)-intensity interplay within each spectral range. Precisely, the relative strengths of the TO Raman signals in the Zn–Te and Be–Te spectral ranges, and of the individual TO contributions within each spectral range, are indicated within brackets. The location of the low frequency mode is schematically indicated within each spectral range (dotted lines) for clarity. The star refers to parasitical resonance-induced scattering by the $2LO_{Zn-Te}$ mode. In the inset the Zn–Te signal at $x = 0.09$ is enlarged for clear insight upon the low frequency mode, marked by an arrow.

While the stiff Be–Te bond exhibits a clear one-bond → two-mode behaviour, there is an apparent one-bond → one-mode behaviour in the spectral region of the soft Zn–Te bond. However, close examination reveals an additional mode on the low frequency side of the ZnTe-like mode (at ∼174 cm^{-1}), as expected. The extra mode shows up clearly even at low Be incorporation (refer to the arrow in the inset of figure 2) and becomes more and more distinct as the Be content increases. It is not due to the $DALA_{X,L}$ bands, as these were clearly identified far below the spectral region of the Zn–Te optical modes, i.e. at ∼130 and ∼140 cm^{-1}, respectively [20]. The extra mode has a TO character since it is absent from the (LO-allowed, TO-forbidden) Raman spectra obtained in backscattering along the [100]-growth axis of the layers [26]. Thus, the extra mode cannot be from a zone-edge disorder-activated TO band as accounted for by the spatial correlation model [11], because such bands would have little symmetry and show up in all Raman scattering geometries [29].

In terms of both strength and frequency the extra mode (∼174 cm^{-1}) and the dominant TO signal (∼180 cm^{-1}) in the Zn–Te spectral range mirror the weak (∼385 cm^{-1}) and dominant (∼420 cm^{-1}) Be–Te modes, respectively. In particular, the dominant Zn–Te peak continuously blue-shifts for increasing Be content, while the extra mode remains at a fixed frequency for Be content $\leqslant 0.19$, i.e. ∼174 cm^{-1}, and blue-shifts for higher Be content (refer to the dotted guidelines in figure 2). Also, the red-asymmetry of the overall Zn–Te signal, due to the extra mode, increases with the Be content, as expected if the strengths of the extra and dominant Zn–Te TO modes scale as the corresponding Be–Te counterparts, i.e. as x and $1 - x$, respectively [19]. More quantitative support is provided in section 3.3.

Basically, the entire Zn–Te behaviour is similar to the Be–VI reference as outlined in figure 1, including the surprising regime 1 at Be content $\leqslant 0.19$. By analogy, the extra and dominant modes in the Zn–Te spectral range are attributed to the two distinct zone-centre TO

modes corresponding to the Zn–Te vibrations within the minority hard Be-rich region and the dominant soft Zn-rich one, respectively. They are accordingly labelled with superscripts h and s in the following.

3.2. Fractal-like/normal regimes

Now we discuss the nature of regime 1 in (Zn, Be)VI (Be content $\leqslant 0.19$). This is neither bond dependent nor Be dependent, since it is observed not only with the Be–Se and Be–Te bonds, but also with the Zn–Te bond. Remarkably, only the TO^h mode, i.e. the minor TO mode in section 3.1, is concerned in each spectral range. At this stage we emphasize that the frequency of a bond strongly depends on the local neighbourhood. Accordingly, regime 1 must be discussed in relation to the internal structure of the Be-rich hard region at Be content $\leqslant 0.19$. Decisive insight comes from the percolation site theory [15].

By crossing the Be–VI bond percolation threshold a major topological transition occurs. The composite (Zn, Be)VI systems that initially consisted of the two finely interlaced Zn- and Be-rich treelike pseudo-continua (Be content $\geqslant 0.19$) turn into a dispersion of finite Be-rich clusters, with different sizes and shapes, fully embedded within a Zn-rich host matrix (Be content $\leqslant 0.19$). Now, let us consider one of these clusters in particular. A key result of the percolation site theory is that provided this cluster is large enough it has internally a *fractal* geometry. This is reflected by the dependence of its mass on the length scale. The cluster's length is defined by analogy with the radius of gyration R of a complicated polymer and the mass m refers to the number of Be atoms inside. In the case of a homogeneous spherical object m scales as R^3, while for the randomly generated finite clusters m scales as R^d, with $d < 3$ [15]. This simply indicates that the filling of the gyration sphere is not complete; only a fraction of it is occupied by the cluster. Remarkably, all the finite clusters, provided they are large enough, are characterized by the same fractional parameter d [15]. We deduce that all the finite Be-rich clusters, whatever their size in the asymptotic limit, have the same internal geometry. Essentially, when the Be content increases every individual Be-rich cluster expands, but in such a way that the internal structure remains the same. It is within the latter dynamics of individual expansion at fixed internal geometry that the key notion of self-similarity that bridges the scales and carries the concept of fractal in the usual sense comes out.

What emerges is that the Zn–Te and Be–Te bonds within the finite clusters that form the Be-rich dispersion in (Zn, Be)Te at Be content $\leqslant 0.19$ have a stable neighbourhood. This is the very reason why the frequencies of the corresponding TO^h modes in the Raman spectra at Be content $\leqslant 0.19$ are stable. In summary, our view is that regime 1 is a direct indicator of the fractal structure of the Be-rich dispersion (Be content $\leqslant 0.19$), as predicted by the percolation site theory.

Also, the percolation site theory indicates that the fractal character is lost above the percolation threshold, i.e. at Be content $\geqslant 0.19$. The Be-rich treelike pseudo-continuum resulting from the coalescence of the large Be-rich finite clusters becomes a so-called *normal* object [15], in that its internal structure turns smoothly Be dependent. This legitimates *a posteriori* our approach to describe the Be-rich continuum at Be content $\geqslant 0.19$ as a pseudo-ternary alloy whose parent systems consist on one hand of the as-grown percolation cluster at Be content ~ 0.19, thereby viewed as a pseudo-binary compound, and on the other hand of the bulk Be–VI compound (Be content $=1$). On this basis the dependence of the TO^h frequency on the Be content at Be content $\geqslant 0.19$ could be explicitly derived by using a traditional but 'rescaled' MREI description. Details are given elsewhere [18].

Below, regimes 1 and 2 are referred to as the fractal-like and the normal regimes, respectively (refer to figure 1). By symmetry we anticipate a regime 1 for the s-mode at

Be content $\geqslant 0.81$ (refer to figure 1). However, we cannot be conclusive due to the sparse (Zn, Be)Se and (Zn, Be)Te Raman data at this limit [19, 20].

3.3. Soft bonds: simplified version of the percolation model

The above assignment of the one-bond → two-mode behaviour in the Zn–Te spectral range supposes that the Zn–Te bonds are longer within the Be-rich host region than within the Zn-rich one. We discuss this quantitatively by using the first-principles calculations of bond length previously performed by Postnikov *et al* in the fully relaxed $Zn_{26}Be_6Se_{32}$ prototype supercell corresponding to Be content ~ 0.19 [21].

From these calculations not only the Be–Se bonds but also the Zn–Se ones appear to have a bi-modal bond length distribution. This discriminates between Zn–Se bonds involving the Se atoms from the infinite –Be–Se– chain, that can be considered as part of the Be-rich region, and Zn–Se bonds formed with out-of-chain Se atoms, i.e. far from the chain and thereby part of the Zn-rich region. As expected, the former bonds actually appear to be longer than the latter. The difference is ∼1% [21]. Basically, the infinite –Be–Se– chain has its period fixed by the large lattice constant of the surrounding ZnSe-like crystal. This can be achieved by enlarging the Be–Se interbond angles within the chain, making the zigzag chain straighter [21]. We argue that this longitudinal distortion of the chain generates in turn the observed stretching of the transverse Zn–Se bonds attached to the chain. We expect similar results for (Zn, Be)Te, because the substituting species remain the same.

Remarkably, while the difference in bond lengths between the bonds from the Be-rich and Zn-rich host regions are comparable for the Be–VI (∼2%) and Zn–VI (∼1%) series, the frequency gap between the weak and dominant modes in the TO Raman spectra is much larger for the stiff Be–Te bond [20] (∼40 cm^{-1}, ∼8.5% of the bulk BeTe TO frequency) than for the soft Zn–Te one (∼3 cm^{-1}, ∼1% of the bulk ZnTe TO frequency), by about one order of magnitude. Incidentally, a large frequency gap was also observed for the stiff Be–Se bond in (Zn, Be)Se [19] (∼50 cm^{-1}, i.e. ∼10% of the bulk Be–Se TO frequency), and the stiff Ga–N bond in the highly lattice-mismatched (∼20%) GaAsN alloy [22] (∼47 cm^{-1}, i.e. ∼8.5% of the bulk TO frequency in cubic GaN).

Essentially, the variation in the bond force constant due to change in the bond length, i.e. anharmonic effects, seems exacerbated for the stiff bonds but quasi-non-existent for the soft ones. This is why it is possible to generalize the one-bond → two-mode percolation model developed for the stiff Be–VI bonds in the random (Zn, Be)VI systems to the usual random alloys, i.e. made of only soft-like bonds. In essence the rather complicated one-bond → two-mode Be–VI TO fine structure outlined in figure 1 (refer to the thin lines), characterized by a large frequency gap δ between the two TO modes from the same bond species out of the percolation range, can be viewed as a distortion of a simpler trapeze-like TO fine structure for soft bonds corresponding to the absence of a frequency gap ($\delta \sim 0$, refer to the thick lines in figure 1). Below, this is referred to as the simplified version of the percolation model.

At last we notice that the fixed Zn–Te and Be–Te TO^h modes have apparently disappeared at the Be-dilute limit (refer to the top spectrum in figure 2). However, careful examination reveals that the remaining Zn–Te and Be–Te modes exhibit marked low frequency asymmetries. We have checked that this is also true for the Be–Se mode in (Zn, Be)Se (refer to the top spectrum of figure 2 in [18]). Our view is that in the Be-dilute limit the Be-rich finite clusters get so small that the Be–Se bonds inside eventually behave as isolated bonds regarding the relaxation of the local tensile strain due to the long Zn–Se bonds. More detail is given in section 4.2. This corresponds to a departure from stability of the TO^h mode towards the TO^s mode (refer to the dotted lines in figure 1), which accounts for the observed asymmetries.

Now we discuss briefly the strength aspect. A very general trend is that the strengths from the overall Be–VI and Zn–VI Raman signals in the random $Zn_{1-x}Be_xVI$ alloys scale as the fraction of related oscillators in the crystal, i.e. as x and $(1-x)$, respectively [1, 2]. Now, care must be taken that the signal within each spectral range is bi-modal, i.e. (h, s)-like. Essentially, the strengths of the TO^h and TO^s modes scale as the scattering volumes of the hard Be-rich and soft Zn-rich host regions, i.e. as x and $(1-x)$, respectively [19]. Multiplication of the individual and global weighting factors for each bond species directly provides the population of Zn–VI and Be–VI bonds within the Be-rich and Zn-rich regions at every alloy composition x. This fixes accordingly the balance of strength between the [$(Zn\text{-}VI)^h$, $(Zn\text{-}VI)^s$, $(Be\text{-}VI)^h$, $(Be\text{-}VI)^s$] TO modes in the Raman spectra. Details are reported elsewhere [19].

The TO Raman lineshapes calculated via the percolation model by applying the Hon and Faust treatment to a version of the MREI model generalized to our four-oscillator system on the above frequency/strength basis are superimposed to the data in figure 2. Technical details concerning the model are given in [19]. The only input data in the Be–Te range are the frequency of the ZnTe:Be local mode ($x \sim 0$), i.e. $\sim$410 cm^{-1}, the BeTe-like TO^h frequency at x_{Be-VI}, i.e. $\sim$385 cm^{-1}, the bulk BeTe TO–LO frequencies ($x = 1$), i.e. 461–503 cm^{-1}, the bulk BeTe Faust–Henry coefficient C_{BeTe}, i.e. -0.20 [22], and $\varepsilon_\infty = 6.9$. The corresponding input data in the Zn–Te range are the frequency of the BeTe:Zn local mode ($x \sim 1$), i.e. $\sim$195 cm^{-1} [26], the ZnTe-like TO^h frequency at x_{Be-VI}, i.e. $\sim$174 cm^{-1}, the bulk ZnTe TO–LO frequencies ($x = 1$), i.e. 176.5–205 cm^{-1}, the bulk ZnTe Faust–Henry coefficient C_{ZnTe}, i.e. -0.11 [30], and $\varepsilon_\infty = 7.2$.

The agreement is excellent. No adjustable parameter is needed. The full TO decomposition obtained by using an individual dielectric function for each oscillator is also displayed, for a clear overview on the balance of strength between the individual (h, s) contributions in each spectral range.

What emerges is that the percolation model applies as well to the stiff/short Be–Te bond and to the soft/long Zn–Te bond, i.e. regardless of the bond properties. This is compatible with the fact that percolation behaviours rely upon far reaching topological effects above all else. Moreover, the one-bond $\rightarrow$ two-mode behaviour is observed in the Raman spectra whether the bond vibration is highly localized (Be–Te), due to the very small mass of one substituting species (Be), or extended over several unit cells in the crystal (Zn–Te). Again, this is compatible with a percolation behaviour as percolation effects take place at the mesoscopic scale and are thereby not sensitive to differences at the scale of the unit cell. Basically, the model takes a universal character and should be applicable to other alloys, which we investigate below.

4. (Ga, In)As

A representative challenging system to test the simplified version of the percolation model is (Ga, In)As. The differences between the frequencies of the zone-centre and the zone-edge TO modes are rather small in the parent materials GaAs ($\sim$15 cm^{-1}) [31] and InAs ($\sim$4 cm^{-1}) [32], so that even small fluctuations in the Ga–As and In–As bond lengths should there again give rise to phonon localization. Precisely, the mismatch between the Ga–As ($\sim$2.45 Å) and In–As ($\sim$2.62 Å) bond lengths ($\sim$7%) is as large as in the (Zn, Be)VI references ($\sim$9%), which supposes similarly large local bond distortions at the origin of the one-bond $\rightarrow$ two-mode phonon behaviour. Still, the contrast between the Ga–As ($\sim$41 N m^{-1}) and In–As ($\sim$35 N m^{-1}) bond-stretching force constants has reduced to a standard value ($\sim$14%) [25]. Moreover, these compare rather well to the Zn–Se ($\sim$35 N m^{-1}) and Zn–Te ($\sim$31 N m^{-1}) references [25]. Accordingly, in a first approximation (Ga, In)As can be considered as a usual alloy, i.e. made of soft-like bonds only.

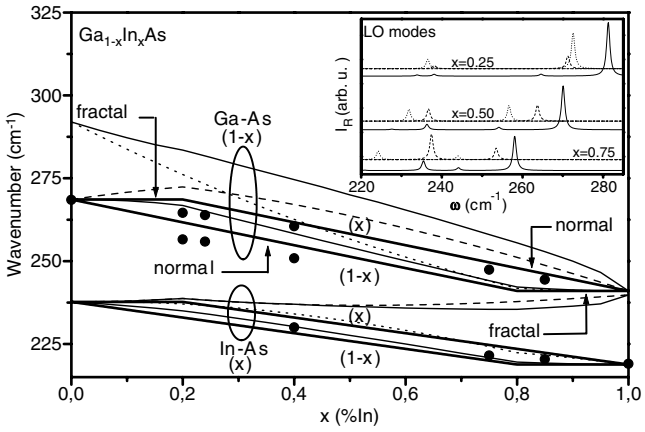

Figure 3. Simplified version of the one-bond → two-mode double branches for the Ga–As and In–As bonds in the random $Ga_{1-x}In_xAs$ alloy. Thick lines refer to TO modes. The relative strengths of the TO Raman signals in the Ga–As and In–As spectral ranges, and of the individual TO contributions within each spectral range, are indicated within brackets. The TO frequencies extracted from the raw spectra in figure 2 of [10] are added, for comparison (plain dots). The dotted, dashed and thin lines refer to the uncoupled LO modes from the Ga- and In-host regions, and to the LO coupled multi-mode, respectively. Examples of the corresponding LO lines at three representative compositions are shown in the inset.

4.1. Simplified version of the percolation model applied to (Ga, In)As

The simplified version of the one-bond → two-mode percolation model ($\delta = 0$, see figure 1) for the TO modes in random (Ga, In)As is displayed in figure 3 (refer to the double pair of thick lines). The whole picture is built up from four empirical parameters only related to the binary compounds, the same as those required to implement the traditional one-bond → one-mode MREI model [1, 2]. These are the bulk TO frequencies in GaAs (268 cm^{-1}) and InAs (218 cm^{-1}), and the frequencies of the impurity modes, i.e. GaAs:In ($x \sim 0$, ~ 237 cm^{-1}) and InAs:Ga ($x \sim 1$, ~ 241 cm^{-1}) [10]. The other input data needed for the calculations of the Raman lineshapes are the (C_{F-H}, ε_∞) values of GaAs (−0.55, 10.9) and InAs (−0.53, 12.3) and the bulk LO frequencies in GaAs (292 cm^{-1}) and InAs (246 cm^{-1}).

The low and high frequency double branches refer to the In–As and Ga–As bonds, respectively. The low and high frequency branches within each double branch refer to vibrations within the randomly formed Ga-rich and In-rich host regions, respectively. The horizontal segments at $x < 0.19$ ($x > 0.81$) refer to the fractal-like regime of the In-rich (Ga-rich) dispersion. The oblique segments at $x > 0.19$ (<0.81) correspond to the normal regime of the In-rich (Ga-rich) continuum. The latter portions are taken as straight lines in a first approximation. In particular, we have checked that the bowing effect associated with the rescaled-MREI description is quasi-negligible in the Ga–As spectral range (not shown) that attracts most of our attention here. This is also true for the In–As double branch. The strength aspect is detailed in section 3.3. The same discussion applies if 'Zn–VI' is replaced with 'Ga–As' and 'Be–VI' with 'In–As'.

The resulting TO Raman lineshapes are shown in figure 4. A small phonon damping of 1 cm^{-1} is taken for a clear overview of the individual modes. In the inset the (Ga, In)As alloy is schematically outlined as a bi-colour composite made of the Ga-rich (white) and In-rich (black) regions, for clarity. In particular the individual TO modes from the In-rich region are

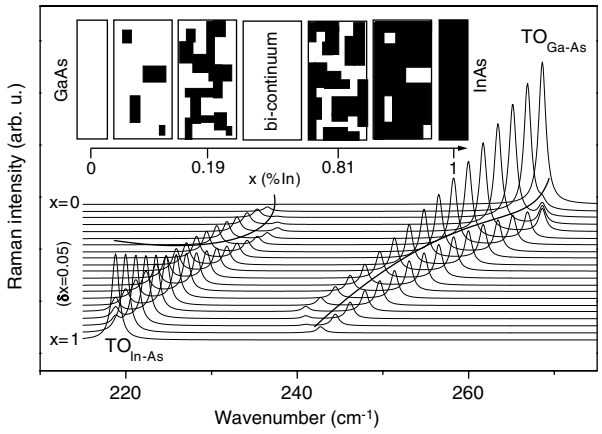

Figure 4. TO multi-modes Raman lineshapes from the $Ga_{1-x}In_xAs$ alloy calculated from the simplified version of the percolation model displayed in figure 3. A small phonon damping of 1 cm^{-1} is taken for a clear overview of the whole phonon system. The individual lines refer to bond vibrations within either the Ga-rich or the In-rich regions from the composite (Ga, In)As alloy. The topologies of the Ga-rich (white) and In-rich (black) regions throughout the whole composition range are schematically represented in the inset. The individual Ga–As and In–As modes from the In-rich region are accordingly labelled for clarity.

accordingly labelled for a clear differentiation. Now let us compare with the available TO Raman data in the literature.

A representative set of TO data from (Ga, In)As covering the whole composition range recently obtained by Groenen *et al* is displayed in figure 2 from [10]. From these data a two-mode behaviour is obvious in the Ga–As spectral range. Groenen *et al* assign the high and low frequency modes as the expected zone-centre Ga–As TO mode (allowed) and a parasitical zone-edge (L) DATO band (theoretically forbidden) as accounted for by the spatial correlation model [11], respectively. However, the low frequency mode is stronger than the high frequency counterpart at small In content, i.e. when the alloy disorder is small. Moreover, the balance of strength turns progressively to the advantage of the high frequency mode when the In content, and thereby the alloy disorder, increase. Both characters seem to exclude such assignment.

Our view is that the low and high frequency modes correspond to two allowed zone-centre Ga–As TO modes originating from the randomly formed Ga-rich and In-rich host regions, respectively. As a matter of fact, the same theoretical TO Raman lineshapes as those reported in figure 4 but with a phonon damping enlarged to a more realistic value of $\sim$10 cm^{-1} reproduce remarkably well the observed Raman lineshapes from figure 2 of [10], as shown in figure 5. We emphasize that no adjustable parameter is used. In particular both the balance of strength and the splitting between the two Ga–As modes are realistic. The In–As double branch is rather flat (see figure 4), so that the two-mode behaviour in the In–As spectral range is screened by the phonon damping, leaving the impression of an apparent one-bond $\rightarrow$ one-mode MREI-like behaviour. For direct insight on the frequencies we have reported in figure 3 the In–As and Ga–As TO frequencies extracted from the raw data in figure 2 of [10] (refer to the dots), for comparison. The overall agreement is rather good in spite of the simplicity of our model.

In essence, we argue that (Ga, In)As obeys the one-bond $\rightarrow$ two-mode percolation model.

Now we discuss briefly the LO modes. These couple via their macroscopic polarization field, with the result that the oscillator strength carried by each individual mode is quasi-fully channelled into a single mode, thereby blue-shifted from the rest of the series. Extensive detail

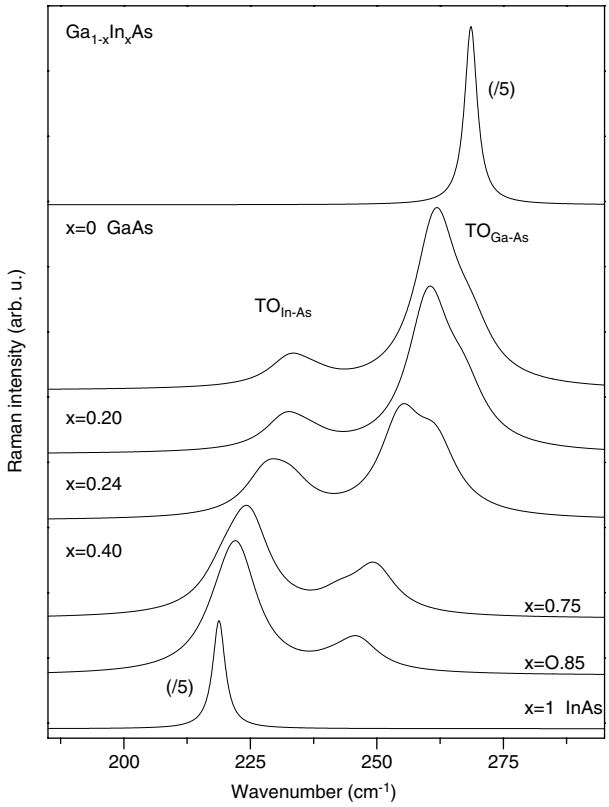

Figure 5. TO multi-mode Raman lineshapes from the $Ga_{1-x}In_xAs$ alloy identical to those reported in figure 4 but with an individual phonon damping enlarged to the realistic value of 10 cm^{-1}, for a direct comparison with the raw TO spectra displayed in figure 2 of [10].

about the process is given in [19]. Accordingly, most of the oscillator strength carried by the low frequency elementary LO In–As (Ga–As) mode is transferred to the high frequency In–As (Ga–As) counterpart from the same double branch, which we refer to as the intra-band transfer. On top of this, a large part of the oscillator strength from the In–As double branch is in turn transferred to the Ga–As double branch, which we refer to as the inter-band transfer. Basically, intra-band transfers superimpose on the inter-band transfer. These are all the more efficient that they address individual modes with close frequencies, and that the oscillator strength is already carried by the higher energy mode [19]. For clear insight, we have superimposed in the inset of figure 3 the uncoupled LO lines (dotted and dashed) derived by using individual dielectric functions for each of the four oscillators predicted by the percolation model [2(In–As), 2(Ga–As)] on the overall LO multi-mode (plain line) obtained by using a single dielectric function for the whole set of oscillators (coupled oscillators). This was realized at representative x-values covering the whole composition range. The full variations of the corresponding frequencies versus the alloy composition x are accordingly reported in the body of figure 3. In particular, we notice a typical coupling-induced anticrossing effect in the Ga–As band at $x \sim 0.3$.

Now, we discuss briefly the peculiar behaviours observed in the LO Raman spectra in the light of the percolation model. One general feature is that the intra-band transfers lead to a misleading one-bond $\rightarrow$ one-mode LO behaviour within each of the In–As and Ga–As spectral ranges (refer to $x = 0.5$ and 0.75 in the inset of figure 3). In particular the intra-band

transfer within the (Ga–As) double branch explains why the low frequency Ga–As LO mode in the Raman spectra remains weak, and is repelled close to the corresponding TO mode at any x (see section 1). The latter behaviour explains why Mintairov *et al* have detected a very small TO–LO splitting for the extra Ga–As mode at $x \sim 0.25$ by infrared analysis [9]. Finally, the inter-band transfer accounts for the spectacular strength of the dominant Ga–As LO mode at large x (refer to $x = 0.75$ in the inset of figure 3). In particular we have checked that at $x \sim 0.95$ the LO response consists of apparent In–As and Ga–As features with similar intensities, as is actually observed [10]. Further discussion of the LO modes is beyond the scope of this work.

Basically, the percolation model accounts for all the apparent anomalies of the TO and LO signals in Raman/infrared analysis. Also, it clearly appears that the strength/frequency information is corrupted in the LO symmetry due to the coupling via the long range longitudinal polarization field. This justifies *a posteriori* our focus on the percolation behaviour, mainly on the TO modes.

More generally, our view is that in most random zinc-blende alloys flat TO double branches and LO intra-band transfers of oscillator strength combine so as to leave the misleading impression of a one-bond → one-mode MREI-like behaviour in the Raman/infrared spectra.

4.2. Bond length distribution in (Ga, In)As

Postnikov *et al* have verified that the microscopic mechanism responsible for the one-bond → two-mode behaviour in the TO Raman spectra of (Zn, Be) chalcogenides is the difference in bond length according to whether the bonds belong to the Zn-rich or Be-rich regions [21]. On this basis the one-bond → two-mode behaviour in the TO Raman spectra comes down to a one-bond → two-mode behaviour in the bond length distribution. Care must be taken that the shorter the bond length, the higher the bond force constant and thereby the frequency of vibration in the Raman/infrared spectra.

Accordingly, in order to validate the percolation picture for $Ga_{1-x}In_xAs$ we need direct evidence that the Ga–As and In–As bonds are longer within the Ga-rich region than within the In-rich region. We consider the critical compositions near the bond percolation thresholds and focus our attention on the minority bond species. Indeed it is easy to figure out the In-rich and Ga-rich regions at these limits. For example, at In content $x \sim 0.8$ the Ga–As bonds within the In-rich and Ga-rich regions ideally correspond to isolated Ga–As bonds and to bonds connected into a pseudo-infinite –Ga–As– chain, respectively. Precisely, the first-principles calculations performed by Postnikov *et al* by using the prototype $Zn_{26}Be_6Se_{32}$ supercell were implemented so as to discriminate between these two extreme situations [21]. For (Ga, In)As we consider a more realistic partition that also takes into account the intermediary situation of bonds connected into finite chains. Basically, we set out to verify that the overall bond length distribution remains bi-modal in character, corresponding to the actual two-mode behaviour in the Raman/infrared spectra.

In order to analyse the variation in bond length of the minority bond species in (Ga, In)As near the bond percolation thresholds, we compute the relaxed atomic positions in a series of large $6 \times 6 \times 6$ supercells that represent In-poor ($x \sim 0.2$) and Ga-poor ($x \sim 0.8$) alloys. We have generated 20 each of In-poor and Ga-poor supercells by positioning atoms randomly in the cell while satisfying the composition, and relaxed their atomic positions. Note that the Ga- and In-poor supercell configurations are exactly the same, except for the fact that Ga and In atoms are interchanged. However, as discussed below the atomic relaxations are quite different between Ga-poor and In-poor cases. For each, we divide the minority cation–As bonds into several categories.

Table 1. Number of bonds of various categories in 20 $6 \times 6 \times 6$ cubic supercells representing random $Ga_{0.24}In_{0.76}As$ and $Ga_{0.76}In_{0.24}As$ alloys.

Infinite chains	Side chains	Isolated bonds	Others (isolated clusters)	Total
25 513	553	1409	15 684	43 159

(1) Isolated cation–As bonds: these are bonds where the next nearest cation is of different type.
(2) Infinite chains: these are bonds that are part of chains that cross the supercell, leaving and entering at the same site, forming an infinite chain.
(3) Side chains: these are bonds connected to one another and eventually to As atoms from the infinite chains, but which themselves are 'dead end' branches of the main infinite chain.
(4) Others: these can be called isolated clusters and are groups of cation–As bonds connected to one another, but not into an infinite chain.

The nominal In contents of 24% and 76% within the percolation range are taken, so that in particular percolation on the minor cation sites is expected. Moreover, as we use large supercells (1728 atoms) we have many bonds of all four types. With lattice constants in pure GaAs and InAs of 5.653 and 6.058 Å, respectively, these compositions result in overall lattice constants of 5.751 and 5.961 Å for the In-poor and Ga-poor systems, respectively. The latter lattice constants correspond to the average bond length of 2.490 and 2.581 Å for the In-poor and Ga-poor systems, respectively. Our atomic relaxation fixes the supercell volume; only the internal coordinates are allowed to relax.

To compute atomic relaxation we use a generalization [33, 34] (generalized VFF, GVFF) of the original [35] valence force field model. The GVFF Hamiltonian (equation (24) in [33]) contains harmonic terms in bond length stretching, bond angle distortion and coupled bond stretching and distortion, and an anharmonic term in bond stretching. The stretching, bending and length–angle interaction coefficients are related to the elastic constants in a pure zinc-blende structure (see equation (25) in [33]).

After atomic relaxation, the bond lengths for the bonds in a supercell in the above categories are calculated and saved. The averaging over all the supercell configurations is accomplished by simply adding up all the bonds of each category together. We then compute a histogram of the overall bond length distribution and plot this distribution. Table 1 lists the total number of bonds in each category. Figures 6 and 7 show the resulting Ga–As and In–As bond length distributions in the (Ga, In)As supercells corresponding to the In contents $x = 0.76$ and 0.24, respectively.

First we focus our attention on the minority Ga–As bonds in the (Ga, In)As supercell corresponding to $x = 0.76$ (figure 6), as clear trends can be observed. The distribution is centred at $\sim$2.49 Å, i.e. the average bond length dictated by the overall lattice constant of the composition. The crucial point is that the isolated Ga–As bonds (1) are shorter ($\sim$1%) than those from the infinite Ga–As chain (2). At first glance this may appear counter-intuitive, as the Ga-rich infinite chain should be more GaAs-like. However, the Ga–As bonds along the infinite chains are restricted by the fixed, composition-determined Vegard lattice constant of the supercell, while the isolated Ga–As bonds are not. That is, the relaxation of the local tensile strain around a zero-dimensional defect, i.e. an isolated Ga atom, is more effective than around a one-dimensional defect, i.e. a pseudo-infinite –Ga–As– chain [21].

Finite –Ga–As– chains (4) are an in-between case. Interestingly, however, these bonds do not bring any intermediary stage between distributions (1) and (2). As a matter of fact,

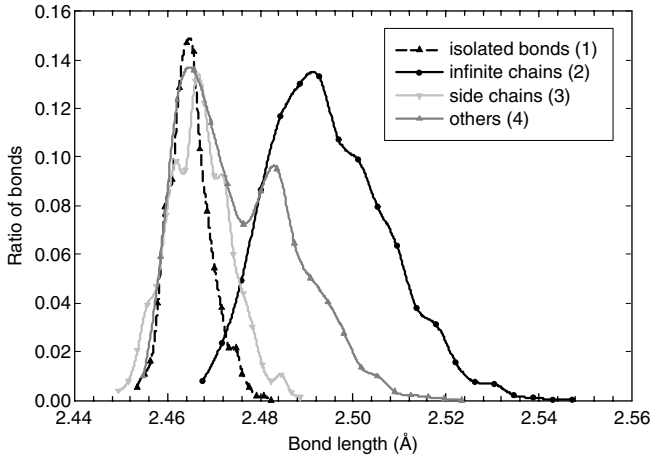

Figure 6. Bond length distributions of the minority bond species in fully relaxed $Ga_{1-x}In_xAs$ $6 \times 6 \times 6$ cubic supercells (1728 atoms) representing Ga-poor ($x = 0.76$) alloys. The different curves distinguish between bonds from isolated cation–As bonds (1), infinite chains (2), chains connected on the side of the main infinite chain (3), and others such as cation–As bonds that form finite chains (4).

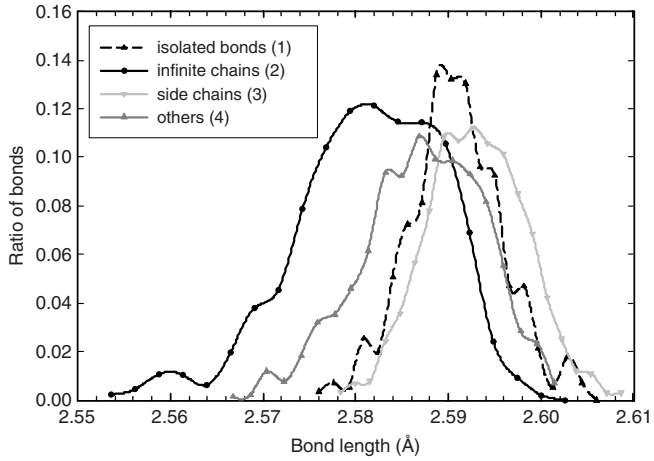

Figure 7. Bond length distributions of the minority bond species in fully relaxed $Ga_{1-x}In_xAs$ $6 \times 6 \times 6$ cubic supercells (1728 atoms) representing In-poor ($x = 0.24$) alloys. The different curves distinguish between bonds from isolated cation–As bonds (1), infinite chains (2), chains connected on the side of the main infinite chain (3) and others such as cation–As bonds that form finite chains (4).

distribution (4) exhibits a marked bi-modal character: some type-(4) bonds behave as zero-dimensional defects, i.e. as type-(1) bonds, and others as one-dimensional defects, i.e. as type-(2) bonds. Intuitively, the set of type-(4) bonds contains both short chains, i.e. nearly type (1), and long chains, i.e. nearly type (2). Finally, the distribution of type-(3) bond lengths, i.e. the side chains of infinite chains, nearly superimposes on distribution (1). We deduce that the Ga–As side chains consist of rather short segments that can also be considered to be zero-dimensional defects in terms of relaxation of the local tensile strain.

Basically, the Ga–As bond length distribution in large supercells that approximate random (Ga, In)As (In content $x \sim 0.8$) has a bi-modal character, as expected. The two modes, located around 2.46 and 2.49 Å, correspond to a rather large difference in bond length of ∼1%. The whole of this is compatible with the observation of a clear bi-modal behaviour in the Ga–As spectral range of the TO Raman spectra from (Ga, In)As. Precisely, a TO splitting as large as ∼9 cm^{-1}, corresponding to ∼3% of the GaAs TO frequency, can be observed at In content $x \sim 0.20$, where the Ga–As signal shows up strongly [10]. For comparison, note that the enlarged splitting of ∼50 cm^{-1} observed between the two Be–Se vibrational modes in (Zn, Be)Se at Be content ∼ 0.20 [19], corresponding to ∼10% of the Be–Se TO frequency, is due to a difference in the Be–Se bond length of ∼2% [21]. The anharmonic effect seems exacerbated for the Be–Se bond, as expected based on the larger bond stiffness of the Be–Se bond than the Ga–As one. This effect is due to a shorter bond length (∼9%) and a higher covalency if we consider the Philips scale (∼3%) [16].

Similar information can be derived for the minority In–As bonds in the (Ga, In)As supercell corresponding to In content $x = 0.24$ (figure 7). However, the overall trend is reversed as the long In–As bonds undergo a local compressive strain from the surrounding GaAs-like host medium, with a smaller lattice parameter. Accordingly, the In–As distribution of bond length is centred at ∼2.58 Å, i.e. the average bond length determined by the overall lattice constant of the composition. The crucial point is that the In–As bonds from the infinite In–As chains (2) are shorter than the isolated ones (1), as expected. Again, this appears counter-intuitive. However, the difference is small, i.e. ∼0.2%, because the In–As bond is not as stiff as the Ga–As one. This accounts for the apparent one-bond → one-mode In–As behaviour in the TO Raman spectra.

What emerges from our atomistic valence force field calculations of the bond lengths around the two bond percolation thresholds in (Ga, In)As is that the minority bonds within the Ga-rich region are longer than those within the In-rich region, with concomitant impact upon the phonon frequencies. This brings strong support to the percolation model for the description of the long-wave phonons in (Ga, In)As.

5. Conclusion

The empirical model based on the percolation site theory initially developed to account for the atypical one-bond → two-mode behaviour of the stiff Be–VI bond in the TO Raman spectra of $Zn_{1-x}Be_x$ (Se, Te) alloys that open the class of random mixed crystals with contrast in the bond stiffness, is here extended to the soft Zn–Te bond in this pioneer system. TO Raman spectra are recorded at increasing Be content up to the limit of detection of the Zn–Te signal, i.e. ∼30%. This provides clear insight into the highly sensitive region of the Be–Te bond percolation threshold ($x \sim 0.19$), where the topology of the Be-rich region changes from a dispersion ($x \leqslant 0.19$) into a continuum ($x \geqslant 0.19$). A one-bond → two-mode behaviour is evident in the Zn–Te spectral range, that mirrors the one-bond → two-mode behaviour in the Be–Te spectral range. In particular, the low frequency mode that refers to the Be-rich dispersion ($x \leqslant 0.19$) has stable frequencies both in the Zn–Te and Be–Te spectral ranges. This is taken as a direct indicator of the fractal structure of the finite clusters that constitute the Be-rich dispersion, as predicted by the percolation site theory.

There remains one major discrepancy between the Zn–Te and Be–Te TO Raman responses: the frequency gap δ between the two TO modes from the same bond species is large for the stiff Be–Te bond but quasi-non-existent for the soft Zn–Te one. However, the differences in bond lengths between the bonds in the Be-rich and Zn-rich host regions are similar for the Be–VI and Zn–VI series. Basically, anharmonic effects seem exacerbated for the stiff bonds

but quasi-non-existent for the soft ones. On this basis, we suggest that in a first approximation δ can be taken equal to zero for the usual alloys, i.e. made of soft-like bonds only.

We use the latter simplified version of the percolation model ($\delta = 0$) to re-examine the much debated multi-phonon behaviour of (Ga, In)As in the Raman/infrared spectra. The lattice mismatch between the parent materials is as large as in (Zn, Be) chalcogenides, which supposes similar local bond distortions, but the contrast in the bond stiffness has vanished. Full contour modelling of the TO and LO Raman lineshapes is achieved within the framework of the percolation model by applying the Hon and Faust treatment to a version of the MREI model generalized to multi-oscillators [2(In–As), 2(Ga–As)]. A random In substitution to Ga is assumed. The theoretical curves are in reasonable agreement with the data taken from the literature, throughout the whole composition range. No adjustable parameter is needed. We conclude that (Ga, In)As obeys the percolation model.

Further, our assignment of the long wave phonons in (Ga, In)As is supported at the microscopic scale by atomistic calculations of the bond lengths for the minority bond species in large supercells that simulate random (Ga, In)As alloys at alloy compositions close to the two bond percolation thresholds, i.e. $\sim$20% and $\sim$80%. The configurations are analysed to distinguish between isolated and in-chain bonds. As expected, a bi-modal behaviour is observed which mirrors the bi-modal behaviour in the TO Raman spectra. In particular the bond lengths of the isolated and connected bonds scale as expected from the percolation model.

According to the percolation picture each $A_{1-x}B_xC$ random alloy consists of a composite system made of the randomly formed A-rich and B-rich regions. Each region brings a specific Raman/infrared signal for each bond species, corresponding to a one-bond $\rightarrow$ two-mode behaviour. The microscopic mechanism is the difference in bond length according to whether the bonds belong to one or the other region. This cannot be achieved by the traditional MREI model based on a VCA description of the crystal. Our view is that the one-bond $\rightarrow$ one-mode MREI-like behaviour evident in the Raman/infrared spectra of most random zinc-blende alloys is apparent only, due to an overdamping, in the broad sense of the term, of the actual one-bond $\rightarrow$ two-mode percolation behaviour.

On the practical side, the percolation picture might renew interest in some zinc-blende mixed crystals, as multi-mode behaviour in the Raman/infrared spectra is usually considered as abnormal, the result of a rather poor crystalline quality or of non-random atomic substitution.

Acknowledgment

This work was supported by the Indo-French Center for the Promotion of Advanced Research (IFCPAR project No 3204-1).

References

[1] Chang I F and Mitra S S 1968 *Phys. Rev.* **172** 924
[2] Chang I F and Mitra S S 1971 *Adv. Phys.* **20** 359
[3] Verleur H W and Barker A S Jr 1966 *Phys. Rev.* **149** 715
[4] Verleur H W and Barker A S Jr 1967 *Phys. Rev.* **155** 750
[5] Mikkelsen J C and Boyce J B 1983 *Phys. Rev.* B **28** 7130
[6] Pearsall T P, Carles R and Portal J C 1983 *Appl. Phys. Lett.* **45** 436
[7] Estrera J P, Stevens P D and Glosser R 1992 *Appl. Phys. Lett.* **61** 1927
[8] Shin H K, Lockwood D J, Lacelle C and Poole P J 2000 *J. Appl. Phys.* **88** 6423
[9] Mintairov A M, Mazurenko D M, Sinitsin M A and Yavich B S 1994 *Semiconductors* **28** 866
[10] Groenen J, Carles R, Landa G, Guerret-Piécourt C, Fontaine C and Gendry M 1998 *Phys. Rev.* B **58** 10452
[11] Tiong K K, Amirtharaj P M, Pollak F H and Aspnes D E 1984 *Appl. Phys. Lett.* **44** 122

[12] Branicio P S, Kalia R K, Nakano A, Rino J P, Shimojo F and Vashishta P 2003 *Appl. Phys. Lett.* **82** 1057
[13] McDevitt T L, Mahajan S, Laughlin D E, Bonner W A and Keramidas V G 1992 *Phys. Rev.* B **45** 6614 and references therein
[14] Toulouse G and Pfeuty P 1975 *Introduction au Groupe de Renormalisation et à ses Applications* (Grenoble: Presses Universitaires de Grenoble)
[15] Stauffer D 1985 *Introduction to Percolation Theory* (London: Taylor and Francis)
[16] Vérié C 1998 *J. Cryst. Growth* **184/185** 1061
[17] Neugebauer J and Van de Walle C G 1995 *Phys. Rev.* B **51** 10568
[18] Pagès O, Ajjoun M, Bormann D, Chauvet C, Tournié E and Faurie J P 2002 *Phys. Rev.* B **65** 035213
[19] Pagès O, Ajjoun M, Tite T, Bormann D, Tournié E and Rustagi K C 2004 *Phys. Rev.* B **70** 155319
[20] Tite T 2004 *PhD Thesis* Université de Metz, France
[21] Postnikov A V, Pagès O and Hugel J 2005 *Phys. Rev.* B **71** 115206
[22] Pagès O, Tite T, Bormann D, Tournié E, Maksimov O and Tamargo M C 2003 *Appl. Phys. Lett.* **82** 2808
[23] Tite T, Pagès O and Tournié E 2004 *Appl. Phys. Lett.* **85** 5872
[24] Bellaiche L, Wei S-H and Zunger A 1996 *Phys. Rev.* B **54** 17568
[25] Martin R M 1970 *Phys. Rev.* B **1** 4005
[26] Pagès O, Tite T, Bormann D, Maksimov O and Tamargo M C 2002 *Appl. Phys. Lett.* **80** 3081
[27] Rajput B D and Browne D A 1996 *Phys. Rev.* B **53** 9052
[28] Cardona M, Etchegoin P, Fuchs H D and Molinà-Mata P 1993 *J. Phys.: Condens. Matter* **5** A61
[29] Saint-Cricq N, Carles R, Renucci J B, Zwick A and Renucci M A 1981 *Solid State Commun.* **39** 1137
[30] Cardona M 1982 *Light Scattering in Solids II* vol 60, ed M Cardona and G Güntherodt (Berlin: Springer) p 62
[31] Hellwege K-H, Madelung O, Schulz M and Weiss H (ed) 1982 *Semiconductors: Physics of Group IV Elements and III–V Compounds* Group III, vol 17 (Berlin: Springer) p 234 and 304
[32] Borcherds P M and Kunc K 1978 *J. Phys. C: Solid State Phys.* **11** 4145
[33] Kim K, Kent P R C, Zunger A and Geller C B 2002 *Phys. Rev.* B **66** 045208
[34] Williamson A J, Wang L-W and Zunger A 2000 *Phys. Rev.* B **62** 12963
[35] Keating P 1966 *Phys. Rev.* **145** 637